CrossMark

Characterization of amorphous silica nanofiller effect on the structural, morphological, optical, thermal, dielectric and electrical properties of PVA–PVP blend based polymer nanocomposites for their flexible nanodielectric applications

Shobhna Choudhary[1,2]

Abstract

The biodegradable polymers blend matrix of poly(vinyl alcohol) (PVA) and poly(vinyl pyrrolidone) (PVP) blend (50/50 wt%) dispersed with amorphous silica (SiO_2) nanoparticles based polymer nanocomposite (PNC) films (i.e., (PVA–PVP)–x wt% SiO_2; $x = 0$, 1, 3 and 5) were prepared by the aqueous solution-cast method. These PNC films were characterized by employing the X-ray diffraction, energy dispersive X-ray spectroscopy, scanning electron microscopy, atomic force microscopy, Fourier transform infrared spectroscopy, ultraviolet–visible spectroscopy, differential scanning calorimetry and dielectric relaxation spectroscopy techniques. It is found that the dispersion of nanosize SiO_2 particles in the PVA–PVP blend matrix reduces the size of PVA crystallites and, turns the surface morphology from smooth into porous and relatively rough for the PNC films. The SiO_2 interaction with polymer structure significantly alters the polymer–polymer interactions, reduces the optical band gap and the glass phase transition temperature, and enhances the melting phase transition temperature of the polymer blend films. The dielectric permittivity of the PNC films initially decreases with the increase of SiO_2 contents up to 3 wt%, but at 5 wt% SiO_2 concentration it is found nearly same as that of the pristine polymer blend matrix. The ac conductivity of these PNC films increases with the increase of frequency according to the power law relation. The dielectric permittivity exhibits non-linear increase with the increase of temperature of the PNC film whereas its dc conductivity obeys the Arrhenius behaviour. The dielectric and electrical properties of these PNC films realize their suitability as low-permittivity and low loss novel nanodielectrics for the substrate and insulator in the development of various microelectronic and organo-electronic devices.

1 Introduction

Among the synthetic biopolymers, the poly(vinyl alcohol) (PVA) and poly(vinyl pyrrolidone) (PVP) are environment-friendly, hydrophilic, biodegradable, non-toxic, non-carcinogenic and biocompatible polymers. These polymers are water-soluble and form the optically clear films when they are prepared by the solution-casting method or spin-coating technique. The films of these polymers have high electrical insulation, and therefore, these are frequently used as a gate dielectric for the fabrication of organic field-effect transistors [1–5], as an insulator in Schottky barrier diodes [6] and also in the fabrication of controllably degradable transient electronic antennas [7]. Further, the PVA and PVP are the most preferred polymers as a binder and capping agents for the preparation of optically sensitive materials used in design and fabrication of optoelectronic and, organic electronic devices and the sensors [8–16]. The hydroxyl (–OH) and carbonyl (C=O) functional groups of PVA and PVP, respectively, are highly sensitive with various functional additives and inorganic nanofillers which results in the formation of compatible composite for advanced functional materials.

Besides the numerous technological applications of the individual polymers, the miscible blend of PVA and PVP was extensively investigated for enhancement of its applications in the areas of biomedical [17, 18], thermal conductor [19, 20], optoelectronics [21, 22], semiconductors

✉ Shobhna Choudhary
  shobhnachoudhary@rediffmail.com;
  shobhnachoudhary@niscair.res.in

1 Dielectric Research Laboratory, Department of Physics, Jai Narain Vyas University, Jodhpur 342 005, India

2 CSIR-National Institute of Science Communication and Information Resources, New Delhi 110 012, India

and electrical insulators [23, 24] and the solid polymer electrolytes [25, 26]. Various spectroscopic, thermo-physical, and morphological studies of PVA–PVP blend and its composite materials established that there is the formation of hydrogen bonding between the –OH and C=O groups in the blend matrix which makes the PVA–PVP as a technological useful compatible blend.

In order to optimize the required thermo-physical, dielectric and electrical properties of a polymer matrix based flexible nanodielectric, the inorganic nanoparticles dispersed polymer nanocomposites (PNCs) have been an intense field of investigations [26–39]. The performance of a conventional polymer as a novel dielectric or electrical insulator can be tailored by proper dispersion of a small amount of suitable inorganic nanomaterial in the flexible polymer matrix which integrates the useful properties of both the polymer and nanofiller, and results in a new class of advanced materials called the 'polymer nanodielectrics (PNDs)'. The high dielectric constant and low loss PND material is needed for the flexible type energy storing devices, whereas low dielectric constant and low loss material is suitable for insulator purpose in the microelectronic devices. Besides the required dielectric properties, there is also need of thermal stability with suitable morphology for the realization of high performance of the devices made of these PND materials. Therefore, the investigations on various types of PNDs consisted of different polymers and various nanofillers are in progress in order to explore the improved properties of each PND material. Silica (silicon dioxide; SiO_2) is frequently used as an inorganic nanomaterial for the preparation of PNDs [28, 30, 35, 40, 41]. So far, the SiO_2 dispersed PVA [42–45] and the PVP [6, 8, 46–52] matrices based PNC and PND materials have been characterized by employing numerous experimental techniques. The survey of literature reveals that the fumed SiO_2 nanoparticle reinforced PVA–PVP blend matrix based PNC films (SiO_2 concentration range from 5 to 25 wt%) are recently characterized for flexible organic electronics [35] and also simulated using molecular dynamics method to elucidate the interaction mechanism of nano-SiO_2 in the polymer blend [52].

In this manuscript, the amorphous SiO_2 nanoparticles dispersed PVA–PVP blend matrix based PNC films (i.e., (PVA–PVP)–x wt% SiO_2; x = 0, 1, 3 and 5) are prepared and characterized to explore their applications as flexible PNDs for the microelectronic device applications. The detailed morphological, structural, optical, thermal, dielectric and electrical properties of these PNC materials containing a low concentration of SiO_2 nanofiller have been characterized and examined in depth by considering the polymer–polymer and polymer–nanofiller interactions.

2 Experimental

2.1 Materials

PVA ($M_w = 7.7 \times 10^4$ g mol^{-1}) and PVP ($M_w = 6 \times 10^5$ g mol^{-1}) of Loba Chemie, India, and SiO_2 nanopowder (particle sizes < 15 nm) of Sigma-Aldrich, USA, were used for the preparation of SiO_2 dispersed PVA–PVP blend based PNC films by aqueous solution-cast method. These reasonably high molecular weight (M_w) PVA and PVP are appropriate in the preparation of PNCs owing to their excellent film-forming ability. For the preparation of each sample, initially, equal weight amounts of PVA and PVP were dissolved in deionized water with required heating in separate glass bottles, and subsequently, these polymeric solutions were mixed and then magnetically stirred for 1 h to obtain the homogeneous PVA–PVP blend aqueous solution. The required amount of SiO_2 for its x wt% concentration with respect to the weight of PVA–PVP blend was firstly dispersed in deionized water. After that, the aqueous dispersed SiO_2 was mixed slowly in the PVA–PVP blend aqueous solution under continuous magnetic stirring for 1 h. This homogeneously prepared (PVA–PVP)–x wt% SiO_2 solution was cast on to a poly propylene dish and the same was kept to dry at room temperature which results the PNC film. The PNC films of different SiO_2 concentrations were prepared by the same procedure as discussed above. The thicknesses of the prepared PNC films were found about 0.015 cm. These PNC films were vacuum dried at 40 °C for 24 h prior to their characterizations.

2.2 Measurements

The X-ray diffraction (XRD) patterns of SiO_2 nanopowder and (PVA–PVP)–x wt% SiO_2 films were recorded in reflection mode at scan rate 0.05° s^{-1} using a PANalytical X′pert Pro (MPD) diffractometer of Cu-Kα radiation (λ = 1.5406 Å) operated at 1800 W (45 kV and 40 mA). Scanning electron microscopy (SEM) (Zeiss EVO MA15) equipped with energy dispersive X-ray spectroscopy (EDX) was used for the morphological and element compositions studies of the PNC film. Surface topography of the PNC films was investigated by employing atomic force microscopy (AFM) (Multimode-V Veeco).

Fourier transform infrared (FTIR) spectra of these PNC films were recorded in ATR mode using an Agilent FTIR Cary 630 spectrometer in the wave number range from 400 to 4000 cm^{-1}. The ultraviolet–visible (UV–Vis) absorption spectra of the (PVA–PVP)–x wt% SiO_2 films were obtained in the range 200–800 nm with a UV–Vis–NIR spectrophotometer (Agilent; Cary 5000, USA).

Differential scanning calorimetry (DSC) measurements of the samples were performed on Mettler Toledo DSC 1 STAR^e system. The DSC thermographs of the samples were taken at a scan rate of 5 °C min^{-1} in the temperature range from 40 to 250 °C under the atmosphere of dried nitrogen.

The complex permittivity $\varepsilon^*(\omega) = \varepsilon' - j\varepsilon''$, electric modulus $M^*(\omega) = M'' + jM''$, ac electrical conductivity $\sigma^*(\omega) = \sigma' + j\sigma''$, and impedance $Z^*(\omega) = Z' - jZ''$ spectra of the PNC film were determined from the dielectric relaxation spectroscopy (DRS) measurements. An Agilent technologies 4284A precision LCR meter equipped with 16451B solid dielectric test fixture was used for DRS measurement over the frequency range from 20 Hz to 1 MHz. The temperature of the PNC film sandwiched between the electrodes of dielectric test fixture was controlled by placing the fixture in the microprocessor controlled oven during the DRS measurements.

3 Results and discussion

3.1 XRD patterns of PNC films

Figure 1 shows the XRD patterns of SiO$_2$ nanopowder and (PVA–PVP)–x wt% SiO$_2$ films. The broad and diffused halo centered at $2\theta = 23.5°$ for the SiO$_2$ powder confirms its
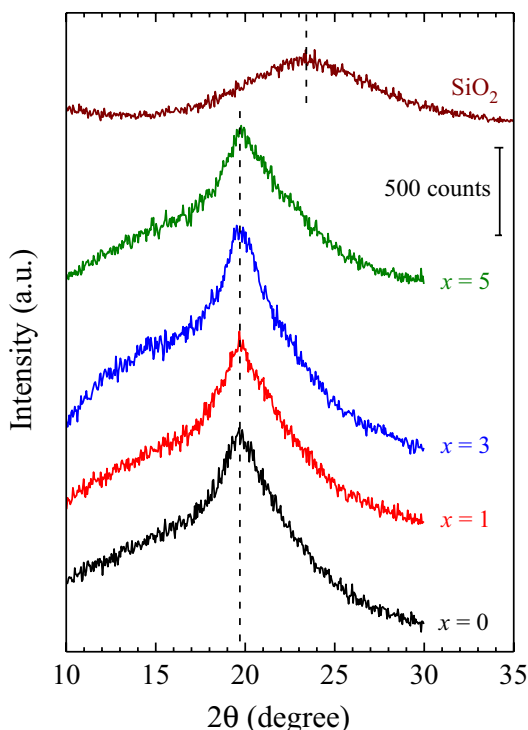

Fig. 1 The XRD patterns of SiO$_2$ nanopowder and (PVA–PVP)–x wt% SiO$_2$ nanocomposite films containing $x = 0$, 1, 3 and 5

amorphous structure. The XRD pattern of (PVA–PVP)–x wt% SiO$_2$ films exhibit broad and slight intense peak around 19.7° which confirms the presence of PVA crystallites in the PNC films. It is because of the pristine PVA which has an intense peak at 19.59° representing its semicrystalline structure, whereas pristine PVP film exhibits broad and diffused halos at 12.04° and 22.5° confirming its amorphous structure [53]. The XRD pattern of the pristine PVA–PVP blend film is found in good agreement with the earlier reported results [53, 54]. The values of 2θ, basal spacing d, crystallite size L and intensity I of pristine PVA and the PNC films were determined from their XRD patterns and the same are given in Table 1. From this table, it can be noted that the relatively low intensity diffraction peak of PVA–PVP blend film ($x = 0$) as compared to that of the pristine PVA peak [53] infers that the intermolecular hydrogen bonding between the PVA and PVP chains in their blend results in huge destruction of PVA crystallites and also decrease their sizes which turns the material into compatible miscible blend. Table 1 shows that the 2θ, d and I values changes anomalously with the increase of SiO$_2$ contents in the PNC films, whereas initially the L value significantly decrease on the dispersion of 1 wt% SiO$_2$ in the PVA–PVP blend film and after that there is a little decrease with the increase of SiO$_2$ content up to 5 wt%. The variation in these structural parameters with the increase of SiO$_2$ concentration in the PNC films reveals that the PVA–PVP blend structures are influenced by the presence of amorphous SiO$_2$ nanoparticles in the blend matrix.

3.2 EDX spectra of PNC films

The EDX characterization of a composite material is mostly attempted for confirmation of the chemical purity and homogeneity of filler particles distribution in the polymer matrix [8, 31, 55, 56]. Figure 2 shows the integrated EDX spectra of (PVA–PVP)–x wt% SiO$_2$ films generated from point scan analysis of the entire area of respective SEM image depicted in the inset of the figure. The analytical composition of each gold sputtered PNC film obtained from the EDX spectra is given in Table 2. The EDX spectrum of PVA–PVP blend

Table 1 Values of Bragg's angle 2θ, basal spacing d, crystallite size L and crystalline peak intensity I of pure PVA, and the PVA crystallite in (PVA–PVP)–x wt% SiO$_2$ nanocomposite (PNC) films

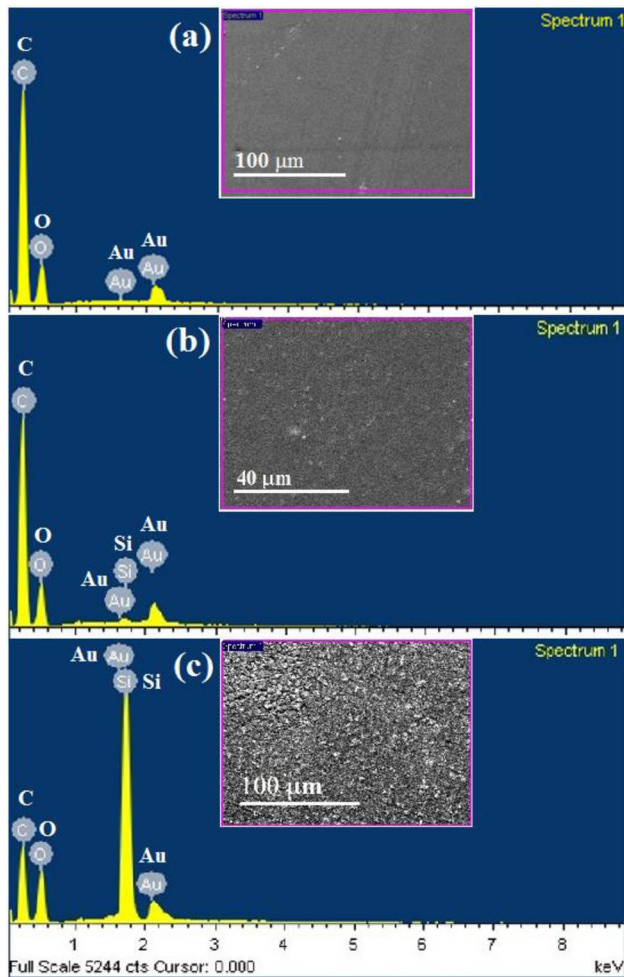| x (wt%)	2θ (°)	d (nm)	L (nm)	I (counts)
Pure PVA film	19.59	0.453	3.87	2969
PVA crystallite in PNC films				
0	19.68	0.451	3.14	632
1	19.72	0.450	2.94	685
3	19.68	0.451	2.89	733
5	19.75	0.449	2.87	578

Fig. 2 The EDX compositional analysis spectra of (PVA–PVP)–x wt% SiO_2 nanocomposite films for **a** $x = 0$; **b** $x = 1$; and **c** $x = 3$

film (Fig. 2a) has energy peaks of carbon (C), oxygen (O) and gold (Au) elements only as expected from the structure of presented elements, and no other element peak was observed which confirm that there are no impurity traces in the sample.

The EDX spectra of SiO_2 containing PNC films (Fig. 2b, c) exhibit the energy peak of Si element in addition to that of the C, O and Au peaks which is also as per expectations for the composite samples, confirming the existence of SiO_2 nanoparticles into the structures of miscible PVA–PVP blend. The composition of C, O, Si and Au elements e.g. weight %, atomic % and compound % along with their chemical formula as obtained from the EDX spectra of these PNC samples are given in Table 2. It is found that the weight % of Si element vary anomalously with the increase of SiO_2 concentration in the PNC samples. But the total percentage values of weight, atomic and compound for each PNC sample was found 100 which can be noted from Table 2. These results infer that there is a significant variation of stabilized nanoparticles in the polymer blend structure going from top to bottom of these solution-cast PNC films. The earlier EDX study on the up surface, fracture and down the surface of the solution-cast PVA–ZnO (95/05) film was also revealed that there is significant variation in the wt% amount of Zn element in the same composition film when it was analyzed at different parts [55]. In addition to this fact, it was further established that only the weight% of elements detected by EDX could not identify exact concentration of the elements in the sample [8], because the absorption within the sample and detector, X-ray induced fluorescence within the sample, surface morphology of the sample, X-ray penetration depth in the sample, and the cross-section of ionization are

Table 2 The electron energy shells corresponding to X-ray emission for the C, Au, O, and Si elements and the values of weight, atomic and compound percentage of these elements along with their chemical formula in the (PVA–PVP)–x wt% SiO_2 polymer nanocomposite (PNC) films obtained from the EDX spectra

Elements	X–ray shell	Weight (%)	Atomic (%)	Compound (%)	Chemical Formula
(PVA–PVP) film					
C	K	26.72	33.22	97.91	CO_2
Au	M	1.86	0.14	2.09	Au_2O_3
O	K	71.42	66.64		
Total (%)		100.00	100.00	100.00	
(PVA–PVP)–1 wt% SiO_2 film					
C	K	26.60	33.15	97.46	CO_2
Si	K	0.10	0.05	0.22	SiO_2
Au	M	2.07	0.16	2.32	Au_2O_3
O	K	71.23	66.64		
Total (%)		100.00	100.00	100.00	
(PVA–PVP)–3 wt% SiO_2 film					
C	K	21.14	27.81	76.70	CO_2
Si	K	9.66	5.48	20.67	SiO_2
Au	M	2.35	0.19	2.63	Au_2O_3
O	K	66.85	66.52		
Total (%)		100.00	100.00	100.00	

several effective factors to be taken into account during the determination of exact concentration of the elements present in the sample.

3.3 SEM images of PNC films

The SEM images of (PVA–PVP)–x wt% SiO₂ films at different scales and magnifications (10 μm and 500 X, 2 μm and 2.0 KX) are depicted in Fig. 3. The SEM image of PVA–PVP blend film confirms it smooth and homogeneous surface (Fig. 3a) which reveals that the blend is miscible, and this SEM is also found in good agreement with that of the same composition blend film SEM image reported earlier [20, 24, 35, 54]. Further, the low scale and high magnification SEM image of this miscible polymer blend (inset of Fig. 3a) exhibits few micro-size cloud-like shapes which may attribute to some novel interfaces of the PVA and PVP miscible phases.

The SEM images of PNC films (Fig. 3b–d) infer that the dispersion of nanosize SiO₂ particles leads to a huge destruction in the surface morphology of the pristine PVA–PVP blend film. Figure 3b shows that the 1 wt% SiO₂ dispersion produces nanosize dips on the surface which can be seen from the high magnification image depicted in the inset of the figure. The nano-size dips over the entire surface

reveal the homogeneity of dispersed SiO₂ particles in the PVA–PVP blend structure. The SEM micrographs of 3 and 5 wt% SiO₂ containing PNC films (Fig. 3c, d) show that the surface turned into phase separated structures (as distinguished from the bright and nano to microsize granules) along with pores of nanometer scale (dark spots). Further, from Fig. 3, it can be noted that the number of white dots per unit area increases with the increase of SiO₂ concentration in the PVA–PVP blend matrix which confirms the homogeneous distribution of filler particles throughout the film surface and below it. Insets of Fig. 3c, d infer that some agglomerated zones of filler particles are formed and their sizes are bigger for 5 wt% SiO₂ containing PNC film.

3.4 AFM images of PNC films

The 2D and 3D AFM images of (PVA–PVP)–x wt% SiO₂ films for their surface topographic analysis are shown in Fig. 4. The gradient of colours and marked scale in the 2D and 3D AFM images confirm a significant variation in the surface topography of the PNC films with the variation of SiO₂ concentrations. The values of surface roughness parameters, namely arithmetic mean roughness R_a and the root mean square roughness R_{rms} of these PNC films, were obtained from the AFM analysis software and listed
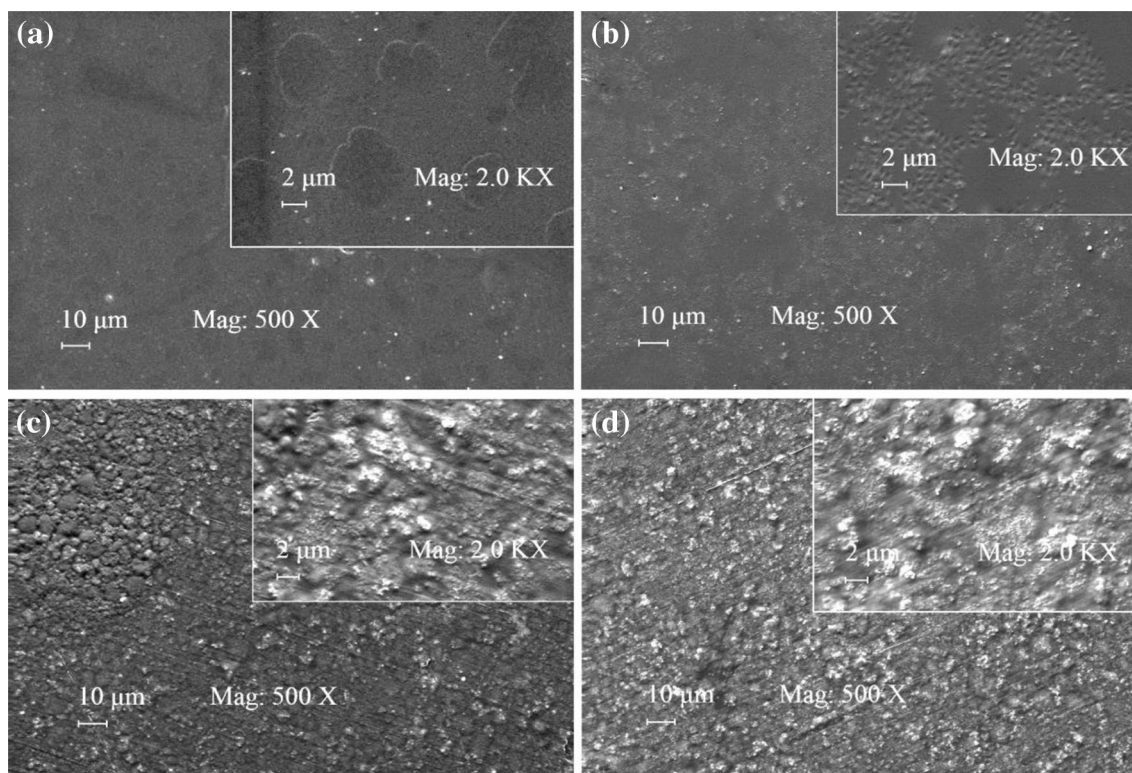

Fig. 3 SEM images of (PVA–PVP)–x wt% SiO₂ films for **a** x=0; **b** x=1; **c** x=3 and **d** x=5 at 10 μm scale with 500 X magnification. Insets show the SEMs of these PNC films at 2 μm scale with 2.0 KX magnification
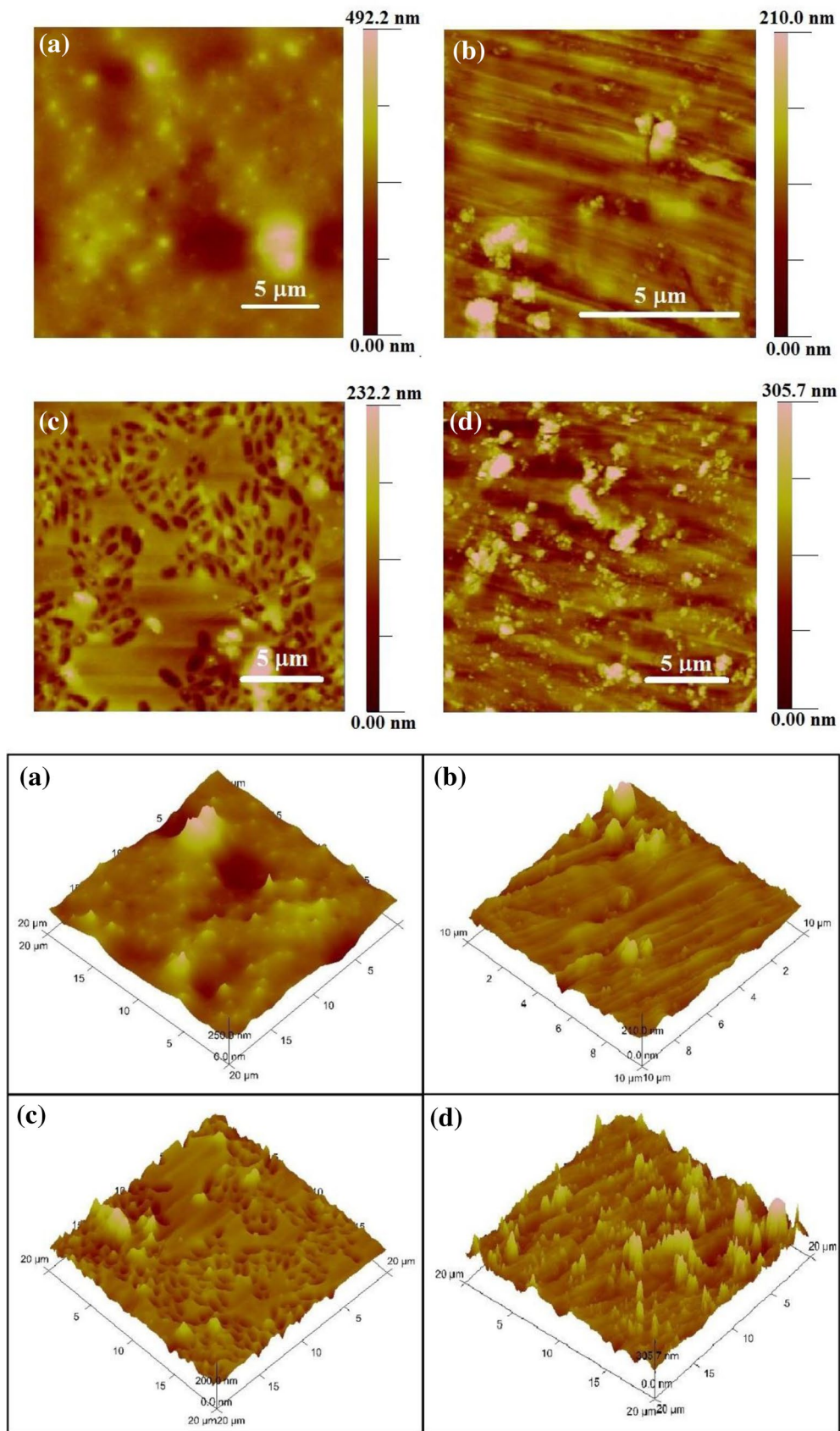
Fig. 4 The 2D and 3D AFM images of (PVA–PVP)–*x* wt% SiO$_2$ nanocomposite films for **a** *x* = 0; **b** *x* = 1; **c** *x* = 3 and **d** *x* = 5

Table 3 Values of surface roughness parameters namely arithmetic mean roughness R_a, the root mean square roughness R_{rms}, and $R_{rms} - R_a$ for the (PVA–PVP)–x wt% SiO_2 films

x (wt%)	R_a (nm)	R_{rms} (nm)	$(R_{rms} - R_a)$ (nm)
0	27.7	42.6	14.9
1	14.9	22.7	7.8
3	17.4	25.1	7.7
5	29.9	46.7	16.8

in Table 3. From this table, it is observed that the values of R_a and R_{rms} vary anomalously with the increase of SiO_2 contents in the PVA–PVP blend film. The R_a and R_{rms} values of 1 wt% SiO_2 containing PNC film are found about one-half that of the pristine PVA–PVP film. For the 3 wt% SiO_2 containing PNC film, the R_a and R_{rms} values slightly increase, whereas these parameters largely increase for 5 wt% SiO_2 containing PNC film and become higher than that of the pristine PVA–PVP blend film. Table 3 shows that the $R_{rms} - R_a$ values of 1 and 3 wt% SiO_2 containing PNC films are exactly same but these are about half of the pristine PVA–PVP film which indicates the strong interfacial interactions and high adhesion between the SiO_2 nanoparticles and polymer chains in these PNC films. The relatively increased values of R_a, R_{rms}, and $R_{rms} - R_a$ for the 5 wt% SiO_2 containing PNC film confirms its high surface roughness due to some agglomeration of the dispersed nanofillers in the blend matrix. From these roughness parameters, it can be concluded that the 1 and 3 wt% SiO_2 containing PNC films have relatively smooth surfaces and confirm the suitability to use them as substrate and insulator for fabrication of the microelectronic devices.

3.5 FTIR spectra of PNC films

Figure 5 shows the FTIR spectra of (PVA–PVP)–x wt% SiO_2 films. The FTIR spectrum of pristine PVA–PVP blend film having compositional ratio 50/50 wt% (i.e., at $x = 0$ wt%) exhibits all the characteristic vibrational modes of the pristine PVA [11, 20, 54, 56] and the PVP [20, 54, 56] films with some relative changes in the intensities and positions confirming the miscibility of these polymers due to formation of hydrogen bonding between their hydroxyl (OH) and carbonyl (C=O) functional groups (C=O···H–O). The wavenumbers corresponding to the peaks of various absorption bands of the PVA–PVP blend are marked in the figure. The highly broad band of moderate intensity peak centered around 3291 cm^{-1} attributed to the –OH stretching vibration of PVA, whereas a relatively low-intensity band centered around 2918 cm^{-1} represents the C–H asymmetric stretching vibration mode of both the PVA and PVP molecules. In addition to these broad vibrational modes, the characteristic
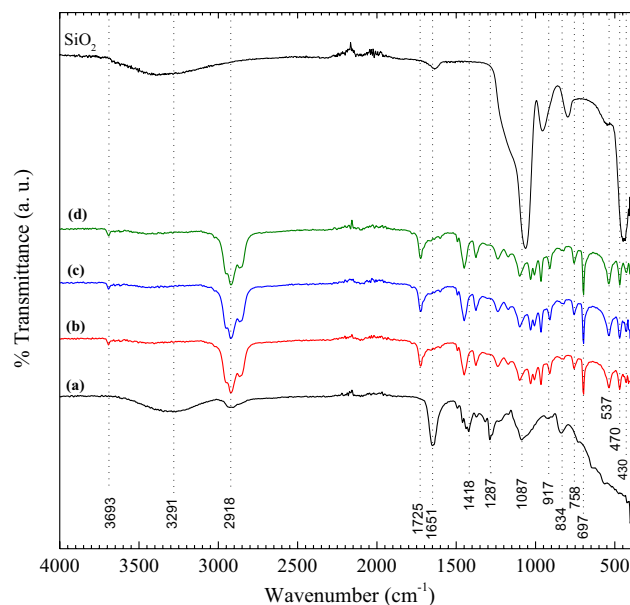
Fig. 5 The FTIR spectra of (PVA–PVP)–x wt% SiO_2 nanocomposite films for (a) $x = 0$; (b) $x = 1$; (c) $x = 3$ and (d) $x = 5$; and also for the SiO_2 nanopowder

band of the C=O stretching vibrational mode of the PVP has an intense and sharp peak at 1651 cm^{-1}. The CH$_2$ wagging and asymmetric twisting modes of these polymers exhibited absorption bands at 1418 and 1287 cm^{-1}, respectively. Further, the absorption peaks appearing at 1087 and 834 cm^{-1} are corresponding to the C–O and C–C vibrational modes of the PVA and PVP chains. A weak absorption band at 1500 cm^{-1} refers to the characteristic vibration of C=N (pyridine ring) of PVP. All these vibration bands of the PVA–PVP blend film are found inconsistent with their literature values [25, 35, 54, 56, 57]. FTIR spectrum of amorphous SiO_2 powder shown in Fig. 5 has characteristic strong absorption bands at 1060 and 450 cm^{-1} corresponding to Si–O–Si chain stretching vibration (O atom motion between two Si atoms) and Si–O bending vibrational mode, respectively. In addition to these bands, the absorption bands for SiO_2 observed at 950 and 800 cm^{-1} represents the bending vibration of Si–OH and the stretching mode of the motion of Si atoms between the two O atoms, respectively. Further, the weak absorption band at 1625 cm^{-1} originates from the –OH bond twisting vibrations of silanol group (Si–OH), whereas, the weak and broadband centered at 3400^{-1} attributed to the extended vibration of the silanol group. These absorption bands of SiO_2 are in good agreement with the earlier studies [58–60].

From Fig. 5, it can be noted that on the dispersion of 1 wt% SiO_2 nanoparticles in the PVA–PVP blend matrix, the intensities of all the characteristic bands of the blend reduces and their position significantly changed. Further, a large number of additional bands have appeared and these

remain unaltered with further increase of SiO_2 contents up to 5 wt%. The FTIR spectra of these PNC films confirm the strong interactions occurred between the SiO_2 nanoparticles and the miscible chain structures of the PVA–PVP blend. The intensity of both the characteristic intense bands (1060 and 450 cm^{-1}) of SiO_2 are almost suppressed, and also the broader band (3400 cm^{-1}) corresponding to its extended silanol group have completely disappeared in the FTIR spectra of the PNC films. Further, the appearance of multiple bands in the spectra of PNC films around the position of strong bands of SiO_2 confirms that the number of SiO_2 vibrational modes increase due to the polymer–nanoparticle interactions. In addition to these bands, a strong and sharp absorption band is immersed at 697 cm^{-1} which is absent in the FTIR spectra of PVA–PVP blend and the SiO_2 powder. This band can be assigned to the rocking vibrational mode of the Si–O–Si chain. Furthermore, the intensity of C–H stretching vibration (2918 cm^{-1}) of the PVA and PVP chain greatly increase and the band has changed into doublet which suggests that the polymer–nanoparticle interactions influence the dynamics of entire chain structures of the polymer blend in the PNC films.

3.6 UV–Vis spectra of PNC films

The UV–Vis absorbance spectra of (PVA–PVP)–x wt% SiO_2 films are shown in Fig. 6. The fundamental intense absorption in the lower wavelength with a sharp edge at about 240 nm was exhibited in these spectra. The absorption edge of these PNC films shifted anomalously towards higher wavelength region with increasing SiO_2 contents up to 5 wt%. These changes in the absorption edge confirm the variation in optical energy band gap of the PNC materials with a change in SiO_2 concentration. The absorption edge of
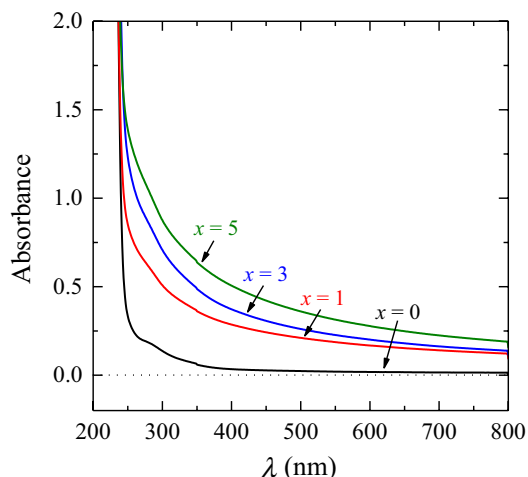

Fig. 6 UV–Vis absorbance spectra of (PVA–PVP)–x wt% SiO_2 nanocomposite films containing $x = 0$, 1, 3 and 5

PVA–PVP blend represents the $\pi \rightarrow \pi^*$ electronic transition [54, 57, 61–63]. The optical parameters namely optical band gap, the Urbach energy and the refractive index of the PNC films were determined using the various relations demonstrated earlier [62, 64–68] in order to understand the optical behaviour of these composite materials in depth.

The various optical energy band gaps E_g of the PNC films were determined using Eq. (1);

$$(\alpha h\nu)^m = B(h\nu - E_g) \tag{1}$$

where α is the absorption coefficient, h is the Plank's constant, ν is the frequency of incident light wave, $h\nu$ is the photon energy, B is a constant and m is a variable ($m = 1/2$, 2, 3/2 and 3 corresponding to the allowed indirect, allowed direct, forbidden direct and forbidden indirect transitions, respectively). The frequency ν dependent values of α were calculated from the frequency dependent absorbance A values of the film and its thickness t_g using the Beer–Lambert's relation;

$$\alpha = 2.303(A/t_g) \tag{2}$$

The A is defined by $\log(I_0/I)$, where I_0 and I are the intensities of the incident and transmitted beams, respectively. For the optical materials, it was established that near the fundamental absorbance edge, both indirect and direct transitions occur, and the energy band gap corresponding to these transitions can be determined by plotting $(\alpha h\nu)^{1/2}$ and $(\alpha h\nu)^2$ as a function of photon energy ($h\nu$).

Figure 7 depicts the $(\alpha h\nu)^2$ versus $h\nu$ and also the $(\alpha h\nu)^{1/2}$ versus $h\nu$ plots for the (PVA–PVP)–x wt% SiO_2 films. The values of direct optical band gap E_{gd} and indirect optical band gap E_{gi} were determined by extrapolating the linear portion of the high energy curves to the photon energy axis at zero absorbance as shown by the solid lines in the respective figures. The observed values of E_{gd} and E_{gi} of the PNC films are reported in Table 4 which are around 5 eV. For these PNC films, their E_{gd} values are found slightly higher than that of the E_{gi}. Further, it is observed that the optical band gap values decrease nonlinearly with the increase of SiO_2 contents up to 5 wt% in the PNC films. The energy band gap values of these PNC films has also been determined from the α versus $h\nu$ plots (inset of Fig. 7a) which are found exactly same as that of the E_{gd} values determined from the $(\alpha h\nu)^2$ versus $h\nu$ plots.

The optical band gap $E_{g(T)}$ of these photon absorbing PNC films was also determined using the Tauc's relation;

$$w^2 A = (hw - E_{g(T)})^2 \tag{3}$$

where $\omega = 2\pi\nu$ and $\nu = c/\lambda$, λ is the wavelength and c (3×10^8 m/s) is the velocity of incident photons. The $E_{g(T)}$
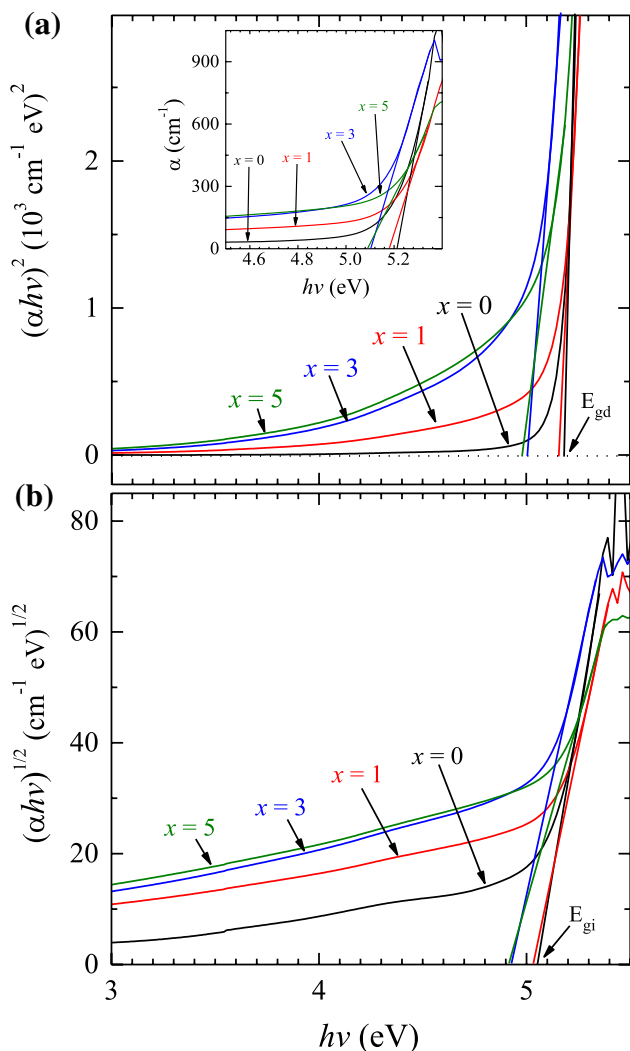
Fig. 7 Plots of **a** $(\alpha h\nu)^2$ versus photons energy $h\nu$, and **b** $(\alpha h\nu)^{1/2}$ versus $h\nu$ for the (PVA–PVP)–x wt% SiO$_2$ nanocomposite films containing $x = 0$, 1, 3 and 5 for the determination of direct (E_{gd}) and indirect (E_{gi}) energy band gaps. Inset of **a** shows the α versus $h\nu$ plots

Table 4 Values of optical energy gap (E_{gi}, E_{gd} determined from Davis and Mott model and $E_{g(T)}$ determined from Tauc's plot), Urbach energy E_u, and refractive index n for the (PVA–PVP)–x wt% SiO$_2$ films

x (wt%)	E_{gi} (eV)	E_{gd} (eV)	$E_{g(T)}$ (eV)	E_u (eV)	n
0	5.05	5.19	5.04	1.93	1.994
1	5.03	5.16	5.02	1.61	1.997
3	4.93	5.00	4.95	1.37	2.011
5	4.92	4.98	4.93	1.35	2.011

values for the PNC materials were deduced from the Tauc's plots ($A^{1/2}/\lambda$ vs. $1/\lambda$) shown in Fig. 8. The intersection of the extrapolated linear portion of the curve gives the value
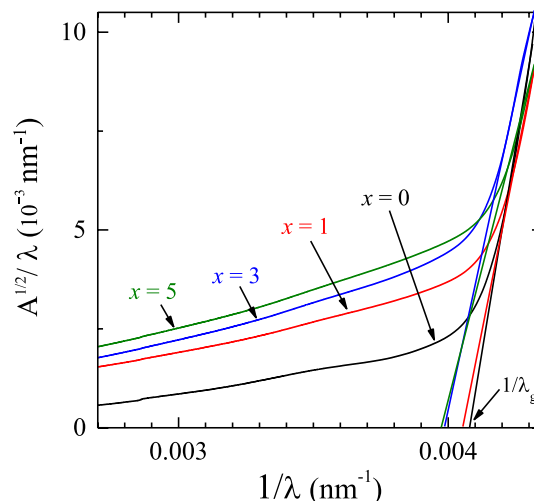

Fig. 8 $A^{1/2}/\lambda$ versus $1/\lambda$ plots of (PVA–PVP)–x wt% SiO$_2$ polymer nanocomposite films

of gap wavelength λ_g from which the $E_{g(T)}$ value was determined using the following relation;

$$E_{g(T)} = hc/\lambda_g \tag{4}$$

The evaluated $E_{g(T)}$ values for these materials are recorded in Table 4. From this Table, it can be noted that the $E_{g(T)}$ values of the studied PNC materials are found equal to that of the E_{gi} values which were determined from the Davis and Mott method.

The refractive index n values for these PNC films were determined from the $E_{g(T)}$ values using the following relation [68];

$$\frac{n^2 - 1}{n^2 + 2} = 1 - \sqrt{\frac{E_{g(T)}}{20}} \tag{5}$$

Table 4 shows that the n values of these PNCs are about 2 which increase non-linearly with the increase of SiO$_2$ concentration up to 3 wt% and approach steady state at 5 wt% SiO$_2$ concentration. This behaviour of n values with increasing SiO$_2$ concentration indicates some changes in interatomic spacing and the packing density with the addition of SiO$_2$ nanoparticles in the PVA–PVP blend matrix.

In general, the decrease in the optical band gap of a composite material with the variation in amounts of its constituents presumes to increase with the degree of disorder in the material. In order to confirm the variation in the degree of disordering in these photon absorbing PNC films, the Urbach energy E_u values were also determined, which is related with the absorption coefficient α by the empirical relation [67, 68];

$$\alpha = \alpha_0 \exp\left(h\nu/E_u\right) \tag{6}$$
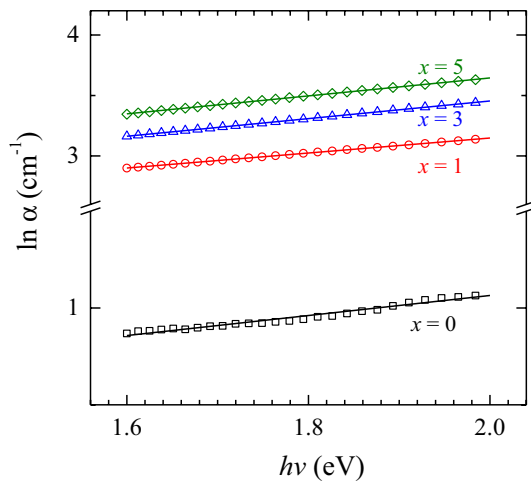
Fig. 9 The ln α versus $h\nu$ plots of (PVA–PVP)–x wt% SiO_2 polymer nanocomposite films

where α_0 is a pre-exponent factor and E_u is the Urbach energy representing the energy bandwidth of the tail of localized states in the band gap. Figure 9 shows that the plots of natural logarithm of the absorption coefficient (ln α) as a function of the photon energy ($h\nu$) for these (PVA–PVP)–x wt% SiO_2 films. It is found that these plots are linear near the fundamental absorption edge which obeys the empirical Urbach relation. The values of E_u of these PNC materials were determined from the reciprocal of the slope of the (ln α) versus $h\nu$ plots, and the observed E_u values are recorded in Table 4. As it can be seen from the Table that the E_u values increase with the increase of SiO_2 concentration in these PNC materials, and this behaviour confirms that the larger the value of E_u there is a greater structural disorder of the material.

3.7 DSC thermograms of PNC films

Figure 10 shows the DSC thermograms for the PNC films which are vertically shifted for better presentation and their scale of heat flow has been marked inside the figure. These DSC curves show intense endothermic peaks in the range 80–100 °C and around 210 °C corresponding to the temperatures of glass phase transition (T_g) and the melting phase transition (T_m) of the PNC materials, respectively. In addition to the prominent melting and glass transition phases, the weak and narrow peak of phase transition centered at 145 °C is also observed which may be attributed to the α-relaxation process associated with the crystalline phases in the films. The highly broad endothermic peak of T_g, whose onset is approximately 55 °C and ends at about 130 °C is apparently a result of the non-uniform nature of this process in the PVA–PVP blend. Further, the exhibited single glass transition temperature of the PVA–PVP blend and its PNC
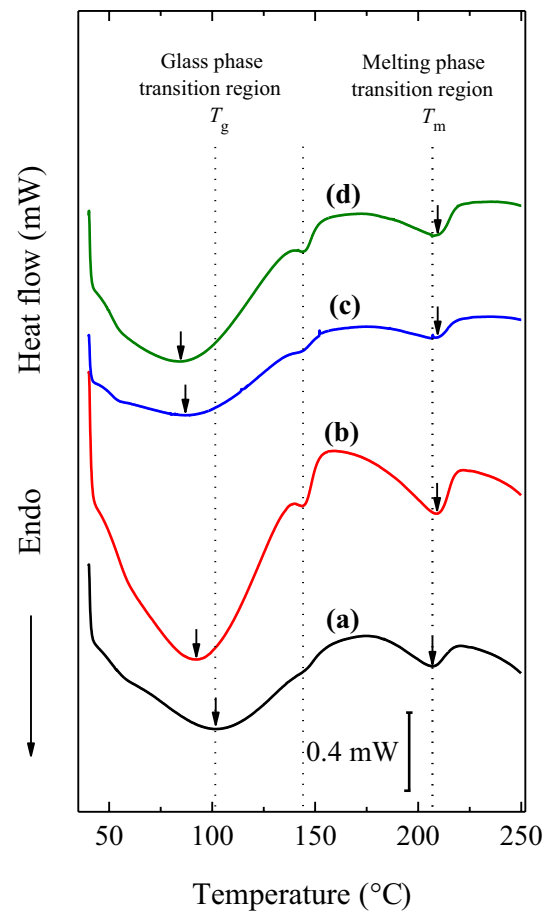

Fig. 10 The DSC thermograms of (PVA–PVP)–x wt% SiO_2 nanocomposite films for (a) $x=0$; (b) $x=1$; (c) $x=3$ and (d) $x=5$

films is an evidence of the blend miscibility, at least in the non-crystalline fraction of the polymer blend.

The values of T_g, T_m and the associated enthalpies (ΔH_g and ΔH_m) of these phase transitions for the PNC films are given in Table 5. The T_g value of the pristine PVA–PVP blend is found in good agreement with the earlier results [24, 57]. From Table 5, it can be noted that the T_g value of

Table 5 The glass phase transition temperature T_g, melting phase transition temperature T_m and the enthalpies of these temperatures (ΔH_g and ΔH_m), and crystallinity X_c of (PVA–PVP)–x wt% SiO_2 films

x (wt%)	Glass phase transition		Melting phase transition		Crystallinity
	T_g (°C)	ΔH_g (J/g)	T_m (°C)	ΔH_m (J/g)	X_c (%)
0	101.38	31.47	206.80	4.48	3.23
1	92.60	45.45	208.70	4.95	3.57
3	86.81	24.50	208.82	1.86	1.34
5	84.21	37.90	208.84	3.19	2.30

the PNC films decreases with the increase of SiO_2 contents in the films which indicates that the SiO_2 contents act as a plasticizer for the used polymer blend matrix. The presence of SiO_2 decreases the polymer network strength and also the heterogeneous intermolecular interactions between the PVA and PVP chains in the blend, thereby leading to decrease of T_g of the PNC films because T_g resulting from micro Brownian motion of the polymer chain backbone. Table 5 shows that the T_m values of the PNC films are about 2 °C higher than that of the pristine PVA–PVP blend film. Further, a gradual increase of T_m values with the increase of SiO_2 contents in the polymer blend matrix confirms the increase in thermal stability of the PNC films which is due to the presence of SiO_2 nanoparticles in the PVA–PVP blend structures. The relative variation in the shape and area of the melting phase transition endothermic peak is attributed to polymer–nanoparticle interactions which influence the melting enthalpy ΔH_m of the phase change. The values of ΔH_m

for the PNC films were determined from the integrated area of the endothermic peak and the observed values of ΔH_m were recorded in Table 5. Using the $\Delta H_{m0} = 138.6$ J/g for the 100% crystallinity X_c of the PVA [18], the X_c values of the PNC films were determined from the relation $X_c = \Delta H_m/\Delta H_{m0}$. The observed X_c values of the PNC films are recorded in Table 5 which anomalously vary with the increase of SiO_2 concentration in the films.

3.8 Dielectric spectra of PNC films

Figure 11 shows the ε′, ε″ and tanδ spectra of (PVA–PVP)–x wt% SiO_2 films over the frequency range from 20 Hz to 1 MHz at 30 °C and also for the (PVA–PVP)–3 wt% SiO_2 film with the temperature variation from 30 to 60 °C. The observed values of ε′ and ε″ represent the electrical energy storing capacity and the energy loss per cycle, respectively in these PNC based 'polymer nanodielectric' (PND)
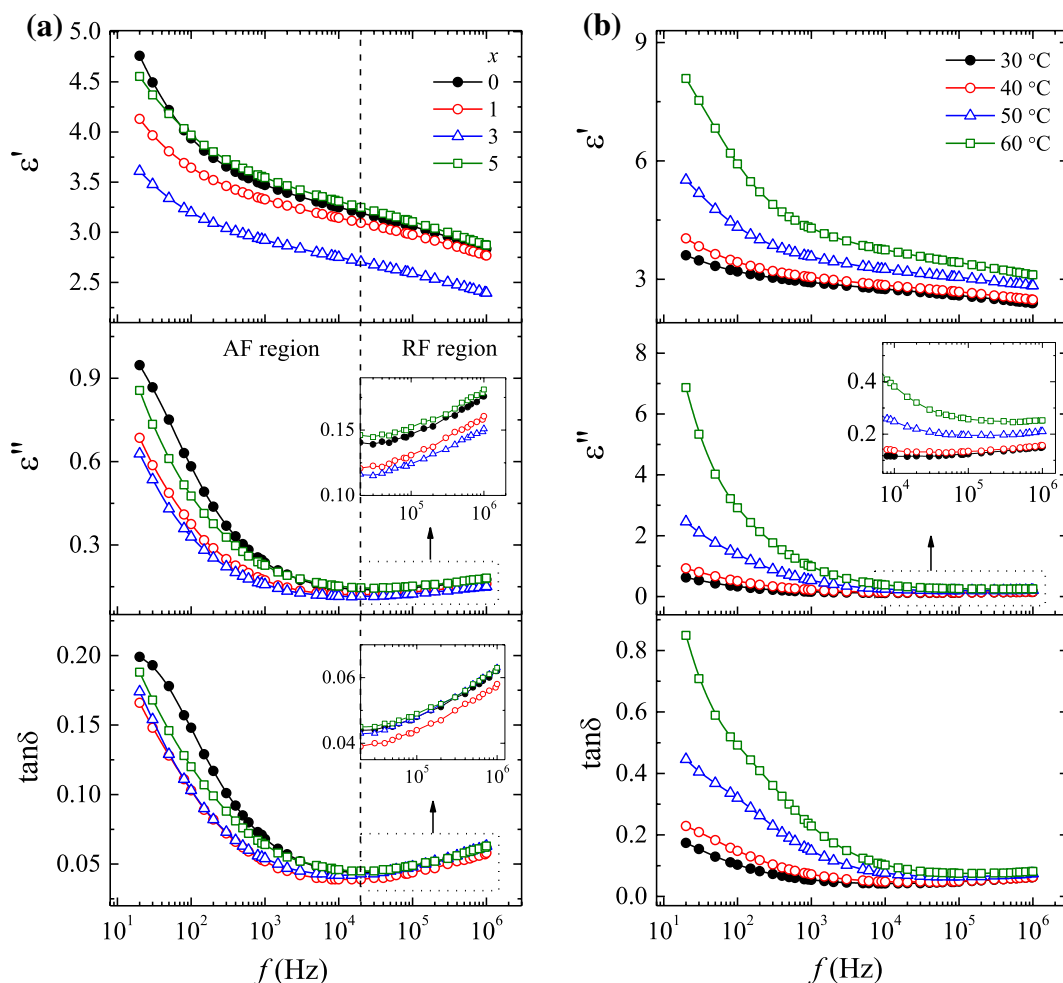

Fig. 11 Frequency dependent real part ε′ and loss part ε″ values of the complex dielectric permittivity, and loss tangent tanδ of **a** (PVA–PVP)–x wt% SiO_2 nanocomposite films containing $x=0$, 1, 3 and 5 at 30 °C, and **b** (PVA–PVP)–3 wt% SiO_2 nanocomposite film at temperatures 30, 40, 50 and 60 °C. Insets show the enlarged view the spectra in the radio frequency (RF) region

materials. The ε' values of these nanodielectrics have a non-linear decrease with the increase of frequency over the entire range of measurements and also vary with the change of SiO_2 concentration and the increase of temperature of the films. But the ε'' and loss tangent ($\tan\delta = \varepsilon''/\varepsilon'$) values of these films sharply decrease with increase of frequency from 20 Hz about to 1 kHz and then approaches minimum in the intermediate frequency range, and after that these values have gradual increase with the increase of frequency in the high-frequency region (enlarged view shown in the inset of Fig. 11). The shape of ε' and ε'' spectra of the PVA–PVP blend is found in good resemblance to the pristine PVA film [69, 70]. These dielectric spectra suggest that the polymer blend matrix containing equal weight amounts of PVA and PVP, the PVA structure mainly govern the dielectric dispersion of the blend. Further, a huge decrease of complex permittivity with the increase of frequency in the audio frequency (AF) region 20 Hz to 20 kHz is owing to interfacial polarization (IP) effect occurring at the interfaces of different conductivity constituents in these composite materials as noted in numerous inorganic–organic based polymer composites [24, 27, 28, 30, 32, 33, 69–71]. Further, the shape of $\tan\delta$ spectra reveals that these materials may exhibit relaxation peaks below 20 Hz and also above 1 MHz corresponding to the IP process and the polymer dipolar reorientation process, respectively.

Figure 12 shows the ε' and ε'' plots as a function of SiO_2 concentration (x wt%) for the (PVA–PVP)–x wt% SiO_2 films and also as a function of temperature for the (PVA–PVP)–3 wt% SiO_2 film at selective frequencies e.g.

100 Hz, 1 kHz, 10 kHz, 100 kHz and 1 MHz. From Fig. 12a, it can be noted that the ε' values of these PNC films have initial decrease with the addition of SiO_2 nanofiller up to 3 wt% and at 5 wt% SiO_2 concentration these values again increase up to that of the pristine PVA–PVP blend film at all the frequencies. These dielectric results reveal that the loading of 1 and 3 wt% SiO_2 in the PVA–PVP blend matrix significantly reduce the number of parallel aligned dipoles in the polymer blend structure which is mainly due to polymer–nanofiller interactions, and hence, there is a decrease in the effective amount of dielectric polarization. The 3 wt% SiO_2 containing PNC film has ε' value less than 2.5 at 1 MHz which confirms its suitability as low permittivity nanodielectric material for the substrate and insulator in the fabrication of micro electronic and electrical devices working at radio frequencies. Further, the ε'' values of these PNC materials are low by more than one order of magnitude as compared to that of the respective ε' values confirming their suitability as low-loss nanodielectric for the fabrication of energy storing micro capacitors workable at the radio frequency electric field. Furthermore, the ε' value of SiO_2 nanopowder is 3.8 at 1 MHz and 27 °C [72] which is comparable to that of the pristine PVA–PVP blend matrix, and therefore, the variation in ε' values of the PNC films with the change of SiO_2 concentration is predominantly due to the polymer–nanofiller electrostatic interactions.

The ε' and ε'' values of the (PVA–PVP)–3 wt% SiO_2 film increase non-linearly with the increase of temperature of the film, and the non-linearity become more pronounced at lower frequencies (Fig. 12b). The temperature dependent

Fig. 12 Plots of SiO_2 concentration dependent ε' and ε'' values of **a** (PVA–PVP)–x wt% SiO_2 nanocomposite films having $x = 0, 1, 3$ and 5 at 30 °C, and **b** temperature dependent ε' and ε'' values of (PVA–PVP)–3 wt% SiO_2 nanocomposite film at several fixed frequencies
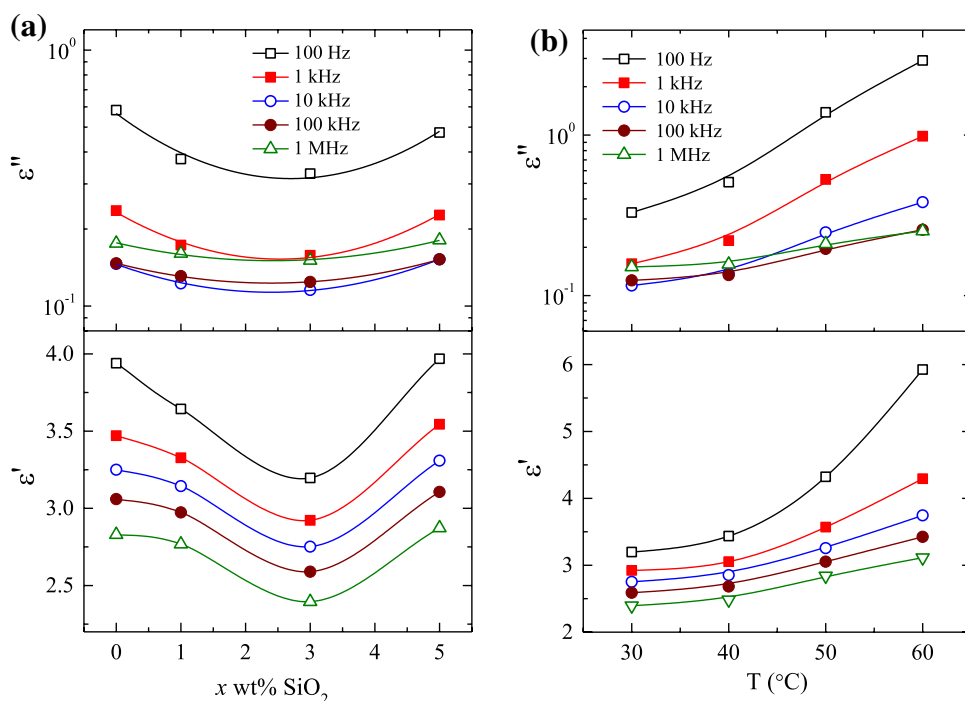
increase of dielectric data confirms the thermally activated dielectric behaviour of the PNC film. Mostly, the increase of temperature creates more free volume in the polymer matrix of composite dielectric material which provide more structural space in regards to ease of dipolar re-orientation and results in enhancement of dielectric polarization (dielectric permittivity values) of the polymeric dielectric materials as confirmed earlier for various PNC materials [23, 30–33, 35, 73–75].

3.9 Electric modulus spectra of PNC films

The electric modulus spectra $M^*(\omega) = 1/\varepsilon^*(\omega)$ of these PNC materials were derived from their frequency dependent ε' and ε'' values. These spectra nullify the contribution of electrode polarization (EP) effect, and the electrode material, the electrode-dielectric contact and adsorbed impurity effects in the composite material [76]. The real part M' and loss part M'' of electric modulus spectra of (PVA–PVP)–x wt% SiO$_2$ films at 30 °C and for (PVA–PVP)–3 wt% SiO$_2$ film with temperature variation from 30 to 60 °C are depicted in Fig. 13. It is found that the M' values of these films increase non-linearly

with the increase of frequency which confirms that the complex permittivity values of these materials reported in Fig. 11 represents the bulk properties because the M' values remain close to zero over the EP effect contributed frequency range. The shape of M'' spectra is found identical to that of the ε'' spectra, and a relaxation peak is exhibited in the lower-frequency-region of the spectra for the PVA–PVP blend film only (Fig. 13a). This relaxation peak may be assigned to the Maxwell–Wagner–Sillars (MWS) relaxation process i.e., the interfacial polarization (IP) effect occurs in the multi-phase composite material. From the comparative shapes of the M'' spectra, it seems that the nanofiller–polymer interactions increase hindrance to this process, and therefore the MWS-relaxation peak for the PNC films shifts towards lower frequencies as compared to the pristine polymer blend film and it has not appeared in the experimental frequency range at room temperature.

The M' and M'' spectra of (PVA–PVP)–3 wt% SiO$_2$ film at temperatures 30, 40, 50 and 60 °C are shown in Fig. 13b. The M' spectra of the PNC film decreases with the increase of temperature, whereas the M'' spectra exhibit the MWS-relaxation peak at 50 and 60 °C. This peak has shift towards high-frequency side as the temperature of the film increases
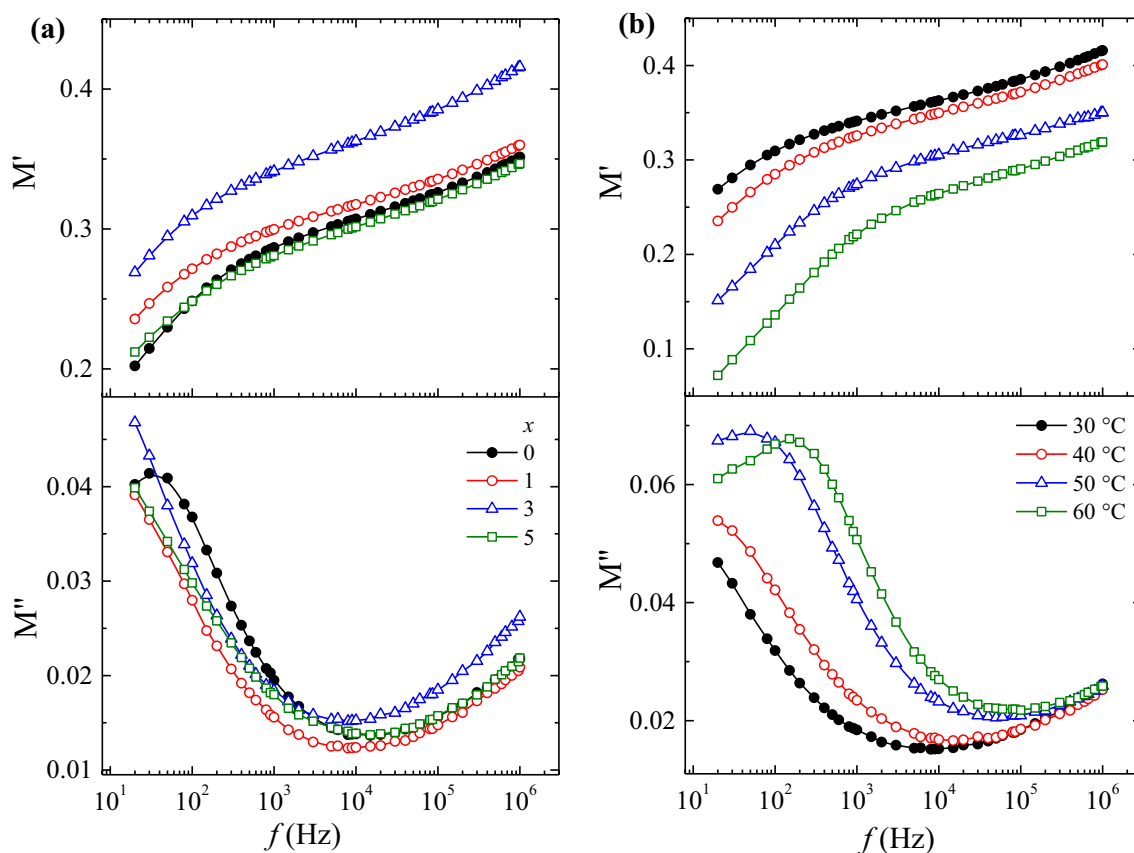

Fig. 13 Frequency dependent real part M' and loss part M'' of complex electric modulus of **a** (PVA–PVP)–x wt% SiO$_2$ nanocomposite films having $x = 0$, 1, 3 and 5 at 30 °C, and **b** (PVA–PVP)–3 wt% SiO$_2$ nanocomposite film at several temperatures

confirming that the PNC film also has the same relaxation process below 20 Hz at 30 and 40 °C.

3.10 AC conductivity and impedance spectra of PNC films

The ac electrical conductivity (σ' and σ'') and the complex impedance (Z' and Z'') spectra of (PVA–PVP)–x wt% SiO$_2$ films, at 30 °C, are shown in Fig. 14. On a log–log scale, σ' and Z' values of these materials have non-linear variation, whereas the σ'' and Z'' values exhibit linear behaviour with unity value of the slope. Further, the σ' and Z' values are found about one order of magnitude lower than that of the corresponding σ'' and Z'' values of these PNC materials. It can be noted from the figure that the low values of conductivity of these PNC materials over the broad frequency range confirm them as novel nanodielectric for an electrical insulator. Further, the magnitude of $Z'' > Z'$ also confirms the
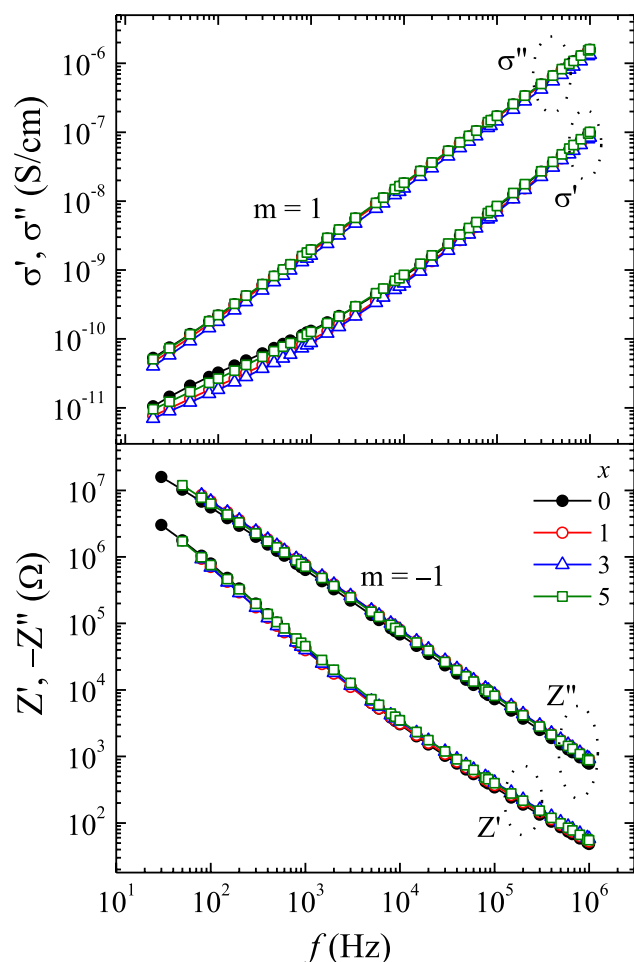
dominant capacitive behaviour of these PNC films which is required for the design of microsize capacitive devices using such type of flexible composite materials.

Figure 15 shows separately the σ' spectra of (PVA–PVP)–x wt% SiO$_2$ films at 30 °C and also of (PVA–PVP)–3 wt% SiO$_2$ film with the temperature variation. These spectra exhibit two clearly distinguishable dispersion regions; firstly over the lower audio frequency (AF) range denoted by region-I and secondly over the intermediate and the radio frequency (RF) range denoted by region-II. This type of conductivity dispersion behaviour of the PNC materials appeared mainly due to their semicrystalline structures [32, 39, 40]. The experimental σ' values of both the regions were fitted to the power law relation $\sigma'(\omega) = \sigma_{dc} + A\omega^n$ where σ_{dc} is the direct current (dc) electrical conductivity, A is a pre-exponential factor and n is a fractional exponent. The σ_{dc} values i.e., $\sigma_{dc(I)}$ and $\sigma_{dc(II)}$, and also the exponent $n_{(I)}$ and $n_{(II)}$ were obtained by power law fit of region-I and region-II, respectively as shown by solid lines separately in the figure. The observed σ_{dc} and n values for these PNC materials are recorded in Table 6. The $n_{(I)}$ values are found significantly lower than unity confirming the hopping mechanism of charges with a long-range translational movement, whereas the $n_{(II)}$ values of these PNC films are found slightly greater than unity confirming that the charge motion involves localized hopping without leaving neighboring sites as discussed for similar type of PNC materials [8]. Further, both the $\sigma_{dc(I)}$ and $\sigma_{dc(II)}$ values of the SiO$_2$ filled these PNC films are found low as compared to that of the pristine PVA–PVP blend film. The temperature dependent conductivity and exponent parameters ($\sigma_{dc(I)}$, $\sigma_{dc(II)}$, $n_{(I)}$ and $n_{(II)}$) for the (PVA–PVP)–3 wt% SiO$_2$ film obtained by power law fit of σ' spectra (Fig. 15b) are also given in Table 6.

Figure 16 shows the plots of $\sigma_{dc(I)}$ and $\sigma_{dc(II)}$ values as a function of SiO$_2$ concentration and also the reciprocal of temperature. From Fig. 16a, it can be noted that the $\sigma_{dc(II)}$ values are more than two orders of magnitude higher than that of the $\sigma_{dc(I)}$ values for these PNC films, whereas these conductivities differ by less than two orders of magnitude for the pristine PVA–PVP blend film (Fig. 16a). These results confirm that the dispersion of SiO$_2$ nanoparticles in PVA–PVP blend matrix produces some hindrance to the charge transport mechanism in the polymeric structures. Further, these conductivity values vary anomalously with an increase of SiO$_2$ concentration in the PNC films. The $\sigma_{dc(I)}$ values of the PNC films are about 10^{-13} S/cm at 30 °C confirming the very high electrical insulation ability of these materials.

Figure 16b shows that the $\sigma_{dc(I)}$ and $\sigma_{dc(II)}$ versus $1/T$ plots are linear confirming the Arrhenius behaviour of temperature dependent conductivity of the (PVA–PVP)–3 wt% SiO$_2$ film. The conductivity activation energy E_σ value of this PNC film was determined from the relation $\sigma_{dc} = \sigma_0 \exp(-E_\sigma/k_B T)$, where
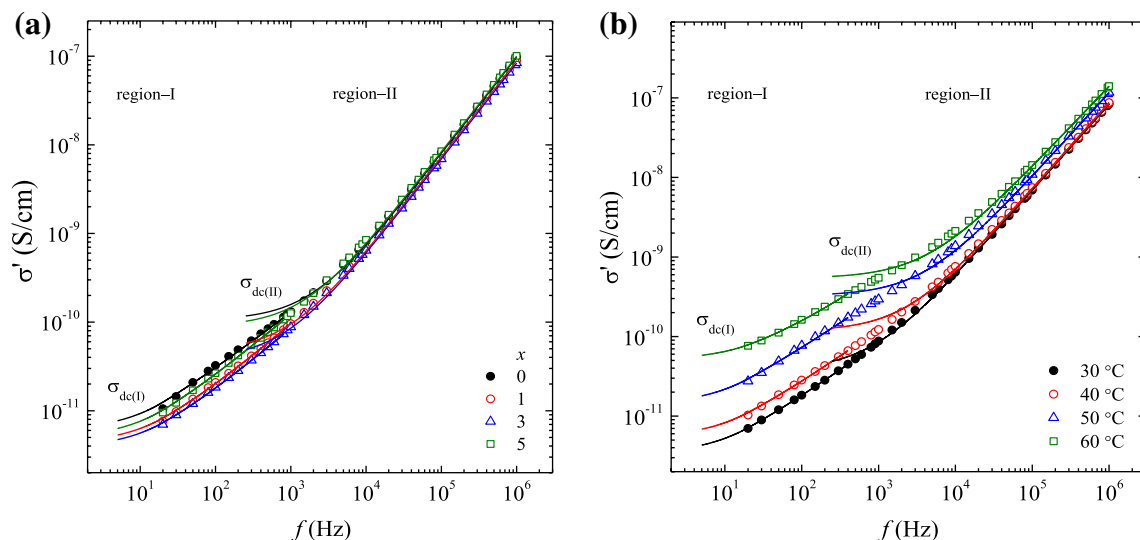

Fig. 14 Frequency dependent real part σ' and loss part σ'' of the complex ac electrical conductivity and the real part Z' and reactive part Z'' of complex impedance of (PVA–PVP)–x wt% SiO$_2$ nanocomposite films containing $x = 0$, 1, 3 and 5 at 30 °C

Fig. 15 Frequency dependent real part σ' of the complex ac electrical conductivity of **a** (PVA–PVP)–x wt% SiO_2 nanocomposite films containing $x = 0, 1, 3$ and 5 at 30 °C, and **b** (PVA–PVP)–3 wt% SiO_2 nanocomposite film at several temperatures. Solid lines show the power law fit $\sigma'(\omega) = \sigma_{dc} + A\omega^n$ of experimental data over low frequency region-I and the high frequency region-II

Table 6 Values of dc electrical conductivities $\sigma_{dc(I)}$ and $\sigma_{dc(II)}$ determined from low frequency and high frequency regions σ' spectra fit to the power law, respectively and their corresponding fractional exponent $n_{(I)}$ and $n_{(II)}$ of the (PVA–PVP)–x wt% SiO_2 polymer nanocomposite (PNC) films at 30 °C, and the (PVA–PVP)–3 wt% SiO_2 film at different temperatures T

PNC films x (wt%)	$\sigma_{dc(I)} \times 10^{12}$ (S/cm) (PVA–PVP)–x wt% SiO_2 films	$n_{(I)}$	$\sigma_{dc(II)} \times 10^{10}$ (S/cm)	$n_{(II)}$
0	2.71	0.66	1.27	1.08
1	1.98	0.69	0.47	1.08
3	1.69	0.69	0.38	1.08
5	2.26	0.70	0.89	1.08
T (°C)	(PVA–PVP)–3 wt% SiO_2 film			
30	1.69	0.69	0.38	1.08
40	2.78	0.68	1.17	1.08
50	8.12	0.66	3.25	1.06
60	26.81	0.64	5.40	1.02

σ_0 is pre-exponent factor, k_B is the Boltzmann's constant and T is the temperature in absolute scale. The evaluated E_σ values corresponding to both the conductivities of the PNC film are marked in the figure which is nearly same i.e., ~0.8 eV. These E_σ values are found in good agreement with the literature values of E_σ for the PVA–PVP blend film ($E_\sigma = 0.78$ eV [77]) and also the nickel chloride filled PVA–PVP blend composite film ($E_\sigma = 0.92$ eV [62]).

4 Conclusions

The PVA–PVP blend matrix dispersed with SiO_2 nanoparticles based polymer nanocomposites (i.e., (PVA–PVP)–x wt% SiO_2; $x = 0, 1, 3$ and 5) were prepared by the solution-cast method. The XRD and EDX studies confirmed that the PNC films are semicrystalline and do not have any kind of impurity traces. The presence of SiO_2 nanoparticles in the PVA–PVP blend matrix significantly modifies the surface morphology and topography of the PNC films. The addition of SiO_2 in the PVA–PVP blend matrix largely destructs the polymer–polymer interactions due to the formation of polymer–nanofiller interactions. The glass phase transition temperature significantly decreases whereas the melting phase transition temperature slightly increases for the PNC films as compared to the pristine PVA–PVP blend film. The optical band gap energy of the PVA–PVP blend film non-linearly decrease with the loading of SiO_2 contents in the PNC films. The complex permittivity and electrical conductivity values
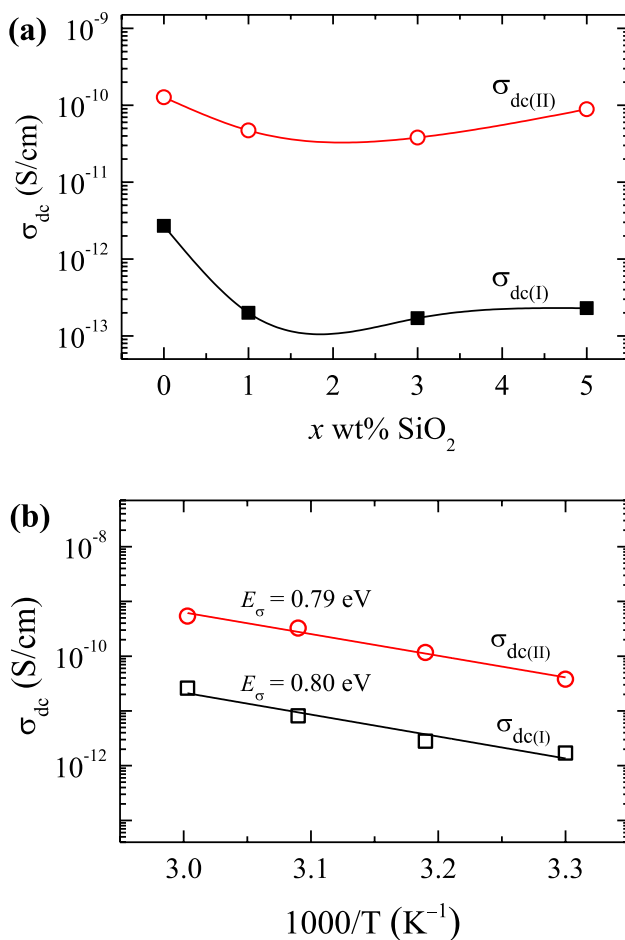
(a)

(b)

Fig. 16 a SiO$_2$ concentration dependent dc conductivity σ$_{dc(I)}$ and σ$_{dc(II)}$ plots of (PVA–PVP)–*x* wt% SiO$_2$ nanocomposite films containing *x* = 0, 1, 3 and 5 at 30 °C, and **b** the Arrhenius plots of dc conductivity σ$_{dc(I)}$ and σ$_{dc(II)}$ of (PVA–PVP)–3 wt% SiO$_2$ nanocomposite film

were found relatively low for 3 wt% SiO$_2$ containing PNC film over the frequency range 20 Hz to 1 MHz. The loss tangent and electric modulus spectra reveal that these PNC films have MWS-relaxation peak below 20 Hz and the polymer chain segment dipolar reorientation relaxation above 1 MHz, at 30 °C. The temperature dependent study of (PVA–PVP)–3 wt% SiO$_2$ film over 30–60 °C exhibit the MWS-relaxation peak in the lower frequency range at temperatures 50 and 60 °C. The temperature dependent dc conductivity of the PNC film obeys the Arrhenius behaviour of activation energy $E_\sigma \sim 0.8$ eV. The complex permittivity (ε′ and ε″) values of the PNC film non-linearly increase with the increase of temperature. The relatively low permittivity and low-loss confirm the suitability of these PNC materials as flexible nanodielectrics for the substrate in microelectronic devices especially fabrication of micro-capacitors, and also electrical insulator in the organic electronic devices. The high amorphous phase of these materials infers their uses as a base matrix in the

preparation of nanocomposite solid polymer electrolytes. The SiO$_2$ concentration dependent optical band gap of these PNC films confirms their uses in band gap tunable optoelectronic devices.

References

1. S. Lee, B. Koo, J. Shin, E. Lee, H.P.H. Kim, Effects of hydroxyl groups in polymeric dielectrics on organic transistor performance. Appl. Phys. Lett. **88**, 162109 (2006)
2. J.S. Choi, Electrical characteristics of organic thin-film transistors with polyvinylpyrrolidone as a gate insulator. J. Inf. Disp. **9**, 35–38 (2008)
3. M. Egginger, M. Irimia-Vladu, R. Schwödiauer, A. Tanda, I. Frischauf, S. Bauer, N.S. Sariciftci, Mobile ionic impurities in poly(vinyl alcohol) gate dielectric: possible source of the hysteresis in organic field-effect transistors. Adv. Mater. **20**, 1018–1022 (2008)
4. E.A. Van Etten, E.S. Ximenes, L.T. Tarasconi, I.S. Garcia, M.M.C. Forte, H. Boudinov, Insulating characteristics of polyvinyl alcohol for integrated electronics. Thin Solid Films **568**, 111–116 (2014)
5. A. Bahari, M. Shahbazi, Electrical properties of PVP–SiO$_2$–TMSPM hybrid thin films as OFET gate dielectric. J. Electron. Mater. **45**, 1201–1209 (2016)
6. M.S.P. Reddy, K. Sreenu, V.R. Reddy, C. Park, Modified electrical properties and transport mechanism of Ti/p-InP Schottky structure with a polyvinylpyrrolidone (PVP) polymer interlayer. J. Mater. Sci.: Mater. Electron. **28**, 4847–4855 (2017)
7. F. Xu, H. Zhang, L. Jin, Y. Li, J. Li, G. Gan, M. Wei, M. Li, Y. Liao, Controllably degradable transient electronic antennas based on water-soluble PVA/TiO$_2$ films. J. Mater. Sci. **53**, 2638–2647 (2018)
8. M. Shahbazi, A. Bahari, S. Ghasemi, Structural and frequency-dependent dielectric properties of PVP-SiO$_2$-TMSPM hybrid thin films. Org. Electron. **32**, 100–108 (2016)
9. S. Sugumaran, C.S. Bellan, Transparent nano composite PVA–TiO$_2$ and PMMA–TiO$_2$ thin films: optical and dielectric properties. Optik **125**, 5128–5133 (2014)
10. S. Sinha, S.K. Chatterjee, J. Ghosh, A.K. Meikap, Analysis of the dielectric relaxation and ac conductivity behavior of polyvinyl alcohol-cadmium selenide nanocomposite films. Polym. Compos. **38**, 287–298 (2017)
11. M. Martin, N. Prasad, M.M. Sivalingam, D. Sastikumar, B. Karthikeyan, Optical, phonon properties of ZnO–PVA, ZnO–GO–PVA nanocomposite free standing polymer films for UV sensing. J. Mater. Sci.: Mater. Electron. **29**, 365–373 (2018)
12. N. Kinadjian, M.F. Achard, B. Julián-López, M. Maugey, P. Poulin, E. Prouzet, R. Backov, ZnO/PVA macroscopic fibers bearing anisotropic photonic properties. Adv. Funct. Mater. **22**, 3994–4003 (2012)
13. A.O. Turkey, A. Barhoum, M.M. Rashad, M. Bechlany, Enhanced the structure and optical properties for ZnO/PVP nanofibers fabricated via electrospinning technique. J. Mater. Sci.: Mater. Electron. **28**, 17526–17532 (2017)

14. B. Karthikeyan, T. Pandiyarajan, R.V. Mangalaraja, Enhanced blue light emission in transparent ZnO: PVA nanocomposite free standing polymer films. Spectrochim. Acta A **152**, 485–490 (2016)

15. T. Pandiyarajan, B. Karthikeyan, Structural, thermal and optical properties of PVP capped ZnO films. Adv. Mater. Res. **678**, 253–257 (2013)

16. M. Kumar, P. Devi, A. Kumar, Structural analysis of PVP capped silver nanoparticles synthesized at room temperature for optical, electrical and gas sensing properties. J. Mater. Sci.: Mater. Electron. **28**, 5014–5020 (2017)

17. B. Choudhuri, B. Mondal, S.K. Ray, S.C. Sarkar, A novel bio-compatible conducting polyvinyl alcohol (PVA)-polyvinylpyr-rolidone (PVP)-hydroxyapatite (HAP) composite scaffolds for probable biological application. Colloids Surf. B **143**, 71–80 (2016)

18. A. Bernal, I. Kuritka, P. Saha, Preparation and characterization of poly(vinyl alcohol) and poly(vinyl pyrrolidone) blend: a biomaterial with latent medical applications. J. Appl. Polym. Sci. **127**, 3560–3568 (2013)

19. X. Xie, D. Li, T.-H. Tsai, J. Liu, P.V. Braun, D.G. Cahill, Thermal conductivity, heat capacity, and elastic constants of water-soluble polymers and polymer blends. Macromolecules **49**, 972–978 (2016)

20. S. Mallakpour, M. Khani, Thermal and morphological studies of poly(vinyl alcohol)/poly(vinyl pyrrolidone)/organoclay nanocomposites containing L-leucine moiety. Colloid Polym. Sci. **294**, 583–590 (2016)

21. I.S. Elashmawi, A.M. Abdelghany, N.A. Hakeem, Quantum confinement effect of CdS nanoparticles dispersed within PVP/PVA nanocomposites. J. Mater. Sci.: Mater. Electron. **24**, 2956–2961 (2013)

22. D. Rithesh Raj, S. Prasanth, T.V. Vineeshkumar, C. Sudarsana-kumar, Ammonia sensing properties of tapered plastic optical fiber coated with silver nanoparticles/PVP/PVA hybrid. Opt. Commun. **340**, 86–92 (2015)

23. A.S. El-Houssiny, A.A.M. Ward, S.H. Mansour, S.L. Abd-El-Messieh, Biodegradable blends based on polyvinyl pyrrolidone for insulation purposes. J. Appl. Polym. Sci. **124**, 3879–3891 (2012)

24. M.T. Ramesan, P. Jayakrishnan, T. Anilkumar, G. Mathew, Influence of copper sulphide nanoparticles on the structural, mechanical and dielectric properties of poly(vinyl alcohol)/poly(vinyl pyrrolidone) blend nanocomposites. J. Mater. Sci.: Mater. Electron. **29**, 1992–2000 (2018)

25. K. Deshmukh, M.B. Ahamed, A.R. Polu, K.K. Sadasivuni, S.K.K. Pasha, D. Ponnamma, M.Al-Ali AlMaadeed, R.R. Deshmukh, K. Chidambaram, Impedance spectroscopy, ionic conductivity and dielectric studies of new Li^+ ion conducting polymer blend electrolytes based on biodegradable polymers for solid state battery applications. J. Mater. Sci.: Mater. Electron. **27**, 11410–11424 (2016)

26. S. Chapi, H. Devendrappa, Optical, electrical, thermal and electrochemical studies of spin-coated polyblend-ZnO nanocomposites. J. Mater. Sci.: Mater. Electron. **27**, 11974–11985 (2016)

27. E. Tuncer, A.J. Rondinone, J. Woodward, I. Sauers, D.R. James, A.R. Ellis, Cobalt iron-oxide nanoparticle modified poly(methyl methacrylate) nanodielectrics: Dielectric and electrical insulation properties. Appl. Phys. A **94**, 843–852 (2009)

28. S. Choudhary, R.J. Sengwa, Dielectric dispersion and relaxation studies of melt compounded poly(ethylene oxide)/silicon dioxide nanocomposites. Polym. Bull. **72**, 2591–2604 (2015)

29. M. Khutia, G.M. Joshi, Dielectric relaxation of PVC/PMMA/NiO blends as a function of DC bias. J. Mater. Sci.: Mater. Electron. **26**, 5475–5488 (2015)

30. M.S. Gaur, A.P. Indolia, A.A. Rogachev, A.V. Rahachou, Influence of SiO_2 nanoparticles on morphological, thermal, and dielectric properties of PVDF. J. Therm. Anal. Calorim. **122**, 1403–1416 (2015)

31. A. Joseph, G.M. Joshi, High performance of fluoro polymer modified by hexa-titanium boride nanocomposites. J. Mater. Sci.: Mater. Electron. **29**, 4749–4769 (2018)

32. S. Choudhary, Dielectric dispersion and relaxations in (PVA–PEO)–ZnO polymer nanocomposites. Phys. B **522**, 48–56 (2017)

33. R.J. Sengwa, S. Choudhary, Dielectric and electrical properties of PEO–Al_2O_3 nanocomposites. J. Alloys Compd. **701**, 652–659 (2017)

34. Y. Zhou, J. He, J. Hu, B. Dang, Surface-modified MgO nanoparticle enhances the mechanical and direct-current electrical characteristics of polypropylene/polyolefin elastomer nanodielectrics. J. Appl. Polym. Sci. **133**, 42863 (2016)

35. K. Deshmukh, M.B. Ahamed, K.K. Sadasivuni, D. Ponnamma, M.A.-A. AlMaadeed, R.R. Deshmukh, S.K.K. Pasha, A.R. Polu, K. Chidambaram, Fumed SiO_2 nanoparticle reinforced biopolymer blend nanocomposites with high dielectric constant and low dielectric loss for flexible organic electronics. J. Appl. Polym. Sci. **134**, 44427 (2017)

36. A. Luzio, F.G. Ferré, F.D. Fonzo, M. Caironi, Hybrid nanodielectrics for low-voltage organic electronics. Adv. Funct. Mater. **24**, 1790–1798 (2014)

37. Z.M. Dang, J.K. Yuan, S.H. Yao, R.J. Liao, Flexible nanodielectric materials with high permittivity for power energy storage. Adv. Mater. **25**, 6334–6365 (2013)

38. Y. Qiao, M.S. Islam, K. Han, E. Leonhardt, J. Zhang, Q. Wang, H.J. Ploehn, C. Tang, Polymers containing highly polarizable conjugated side chains as high-performance all-organic nanodielectric materials. Adv. Funct. Mater. **23**, 5638–5646 (2013)

39. S. Choudhary, R.J. Sengwa, Morphological, structural, dielectric and electrical properties of PEO–ZnO nanodielectric films. J. Polym. Res. **24**, 54 (2017)

40. S. Choudhary, Characterization of SiO_2 nanoparticles dispersed (PVA–PEO) blend based nanocomposites as the polymeric nanodielectric materials. Indian J. Eng. Mater. Sci. **23**, 399–410 (2017)

41. H. Zou, S. Wu, J. Shen, Polymer/silica nanocomposites: preparation, characterization, properties and applications. Chem. Rev. **108**, 3893–3957 (2008)

42. Z. Peng, L.X. Kong, A thermal degradation mechanism of polyvinyl alcohol/silica nanocomposites. Polym. Degrad. Stab. **92**, 1061–1071 (2007)

43. C. Wang, J. Wei, B. Xia, X. Chen, B. He, Effect of nano-silica on the mechanical, thermal, and crystalline properties of poly(vinyl alcohol)/nano-silica films. J. Appl. Polym. Sci. **128**, 1652–1658 (2013)

44. S.J. Lue, S.J. Sheih, Modeling water states in polyvinyl alcohol-fumed silica composites. Polymer **50**, 654–661 (2009)

45. S. Choudhary, R.J. Sengwa, Anomalous dielectric behaviour of poly(vinyl alcohol)-silicon dioxide (PVA-SiO_2) nanocomposites. AIP Conf. Proc. **1728**, 020420 (2016)

46. H. Nakajima, K. Kawano, Preparation and evaluation of the rare earth doped nanoparticle SiO_2–PVP hybrid thin film by sol-gel method. J. Alloys Compd. **408–412**, 701–705 (2006)

47. N. Francolon, A. Potdevin, D. Boyer, G. Chadeyron, R. Mahiou, Luminescent PVP/SiO_2@YAG:Tb^{3+} composite films. Ceram. Int. **41**, 11272–11278 (2015)

48. S.A. Hashemizadeh, Nano organic transistor with SiO_2/poly vinylpyrrolidone dielectric. J. Nanostruct. **6**, 17–22 (2016)

49. A.B. Phatangare, S.D. Dhole, S.S. Dahiwale, V.L. Mathe, S.V. Bhoraskar, D.J. Late, V.N. Bhoraskar, Surface chemical bonds, surface-enhanced Raman scattering, and dielectric constant of SiO_2 nanospheres *in-situ* decorated with Ag-nanoparticles by electron-irradiation. J. Appl. Phys. **120**, 234901 (2016)

50. S. Mallakpour, M. Naghdi, Fabrication and characterization of novel polyvinyl pyrrolidone nanocomposites having SiO_2 nanoparticles modified with citric acid and L(+)-ascorbic acid. Polymer **90**, 295–301 (2016)

51. A. Timin, E. Rumyantsev, S.N. Lanin, S.A. Rychkova, S.S. Guseynov, A.V. Solomonov, E.V. Antina, Preparation and surface properties of mesoporous silica particles modified with poly(*N*-vinyl-2-pyrrolidone) as a potential adsorbent for bilirubin removal. Mater. Chem. Phys. **147**, 673–683 (2014)

52. Q. Wei, Y. Zhang, Y. Wang, M. Yang, A molecular dynamic simulation method to elucidate the interaction mechanism of nano-SiO_2 in polymer blends. J. Mater. Sci. **52**, 12889–12901 (2017)

53. R.J. Sengwa, S. Choudhary, Structural characterization of hydrophilic polymer blends/ montmorillonite clay nanocomposites. J. Appl. Polym. Sci. **131**, 40617 (2014)

54. E.M. Abdelrazek, I.S. Elashmawi, S. Labeeb, Chitosan filler effects on the experimental characterization, spectroscopic investigation and thermal studies of PVA/PVP blend films. Phys. B **405**, 2021–2027 (2010)

55. D.M. Fernandes, A.A. Winkler Hechenleitner, S.M. Lima, L.H.C. Andrade, A.R.L. Caires, E.A. Gómez Pineda, Preparation, characterization, and photoluminescence study of PVA/ZnO nanocomposite films. Mater. Chem. Phys. **128**, 371–376 (2011)

56. B. Kumar, G. Gaur, S.B. Rai, Sensitized green emission of terbium with dibenzoylmethane and 1, 10 phenanthroline in polyvinyl alcohol and polyvinyl pyrrolidone blends. Spectrochim. Acta A: Mol. Biomol. Spectrosc. **187**, 75–81 (2017)

57. E.M. Abdelrazek, I.S. Elashmawi, A. El-khodary, A. Yassin, Structural, optical, thermal and electrical studies on PVA/PVP blends filled with lithium bromide. Curr. Appl. Phys. **10**, 607–613 (2010)

58. A.N. Murashkevich, A.S. Lavitskaya, T.I. Barannikova, I.M. Zharskii, Infrared absorption spectra and structure of TiO_2–SiO_2 composites. J. Appl. Spectrosc. **75**, 730–734 (2008)

59. C. Heng, M. Liu, K. Wang, F. Deng, H. Huang, Q. Wan, J. Hui, X. Zhang, Y. Wei, Biomimic preparation of highly dispersible silica nanoparticles based polymer nanocomposites. Ceram. Int. **41**, 15075–15082 (2015)

60. R.K. Nariyal, P. Kothari, B. Bisht, FTIR Measurements of SiO_2 glass prepared by sol-gel technique. Chem. Sci. Trans. **3**, 1064–1066 (2014)

61. B.M. Baraker, B. Lobo, Dispersion parameters of cadmium chloride doped PVA–PVP blend films. J. Polym. Res. **24**, 84 (2017)

62. H.M. Ragab, Spectroscopic investigations and electrical properties of PVA/PVP blend filled with different concentration of nickel chloride. Phys. B **406**, 3759–3767 (2011)

63. S. Mallakpour, A.N. Ezhieh, Polymer nanocomposites based on modified ZrO_2 NPs and poly(vinyl alcohol)/poly(vinyl pyrrolidone) blend: optical, morphological, and thermal properties. Polym.-Plast. Technol. Eng. **56**, 1136–1145 (2017)

64. E.A. Davis, N.F. Mott, Conduction in non-crystalline systems V. Conductivity, optical absorption and photoconductivity in amorphous semiconductors. Philos. Mag. **22**, 0903–0922 (1970)

65. J. Tauc, Optical properties and electronic structure of amorphous Ge and Si. Mater. Res. Bull. **3**, 37–46 (1968)

66. G.M. Thutupalli, S.G. Tomlin, The optical properties of thin films of cadmium and zinc selenides and tellurides. J. Phys. D **9**, 1639–1646 (1976)

67. F. Urbach, The long-wavelength edge of photographic sensitivity and of the electronic absorytion of solids. Phys. Rev. **92**, 1324–1324 (1953)

68. M.A. Morsi, A.M. Abdelghany, UV-irradiation assisted control of the structural, optical and thermal properties of PEO/PVP blended gold nanoparticles. Mater. Chem. Phys. **201**, 100–112 (2017)

69. R.J. Sengwa, S. Choudhary, Investigation of correlation between dielectric parameters and nanostructures in aqueous solution grown poly(vinyl alcohol)-montmorillonite clay nanocomposites by dielectric relaxation spectroscopy. Express Polym. Lett. **4**, 559–569 (2010)

70. S. Choudhary, R.J. Sengwa, Anomalous behaviour of the dielectric and electrical properties of polymeric nanodielectric poly(vinyl alcohol)–titanium dioxide films. J. Appl. Polym. Sci. **134**, 44568 (2017)

71. R.J. Sengwa, S. Choudhary, S. Sankhla, Dielectric properties of montmorillonite clay filled poly(vinyl alcohol)/poly(ethylene oxide) blend nanocomposites. Compos. Sci. Technol. **70**, 1621–1627 (2010)

72. S. Ketabi, K. Lian, Effect of SiO_2 on conductivity and structural properties of PEO–$EMIHSO_4$ polymer electrolyte and enabled solid electrochemical capacitors. Electrochim. Acta **103**, 174–178 (2013)

73. P. Ilangovan, M.S. Sakvai, A.B. Kottur, Synergistic effect of functionally active methacrylate polymer and ZnO nanoparticles on optical and dielectric properties. Mater. Chem. Phys. **193**, 203–211 (2017)

74. S. Choudhary, Structural, morphological, thermal, dielectric and electrical properties of alumina nanoparticles filled PVA–PVP blend matrix based polymer nanocomposites. Polym. Compos. (2018). https://doi.org/10.1002/pc.24793

75. P.S. Mukherjee, A.K. Das, B. Dutta, A.K. Meikap, Role of silver nanotube on conductivity, dielectric permittivity and current voltage characteristics of polyvinyl alcohol-silver nanocomposite film. J. Phys. Chem. Solids **111**, 266–273 (2017)

76. F.S. Howell, R.A. Bose, P.B. Macedo, C.T. Moynihan, Electrical relaxation in a glass-forming molten salt. J. Phys. Chem. **78**, 639–648 (1974)

77. N. Rajeswari, S. Selvasekarapandian, S. Karthikeyan, M. Prabu, G. Hirankumar, H. Nithya, C. Sanjeeviraja, Conductivity and dielectric properties of polyvinyl alcohol–polyvinylpyrrolidone poly blend film using non-aqueous medium. J. Non-Cryst. Solids **357**, 3751–3756 (2011)